Static Shift Correction and Fractal Characteristic Analysis of Time-Frequency Electromagnetic

Yujian Hou , Qiyun Jiang * , Yan Qiao , Yunsheng Zhao , Zhanxiang He *

Posted Date: 21 February 2025

doi: 10.20944/preprints202502.1721.v1

Keywords: time-frequency electromagnetic; static shift effect; multifractal spectrum analysis

Article

Static Shift Correction and Fractal Characteristic Analysis of Time-Frequency Electromagnetic

Yujian Hou [1,2,3], Qiyun Jiang [3], Yan Qiao [3], Yunsheng Zhao [4] and Zhanxiang He [2,*]

[1] School of Geosciences and Info-Physics, Central South University, Changsha 410083, China
[2] Department of Earth and Space Sciences, Southern University of Science and Technology, Shenzhen 518055 , China
[3] Institue of Urban Underground Space and Energy Studies,The Chinese University of Hong Kong (Shenzhen), Shenzhen 518100, China
[4] Yangtze Delta Region Institute (Huzhou), University of Electronic Science and Technology of China, Huzhou, Zhejiang 313000, China
* Correspondence: hezx@sustech.edu.cn

Abstract: The static shift effect is a distortion in electromagnetic data that severely impacts exploration results. Traditional static effect correction methods are often ineffective, prone to overcorrection or undercorrection, and make it difficult to accurately assess the applicability of the correction. Furthermore, some correction processes require additional data, which increases correction costs. This paper first presents the theoretical foundation for correcting static shift effects in the electric field components using magnetic field component information. Based on time-frequency electromagnetic exploration technology, a method is proposed to correct static shift effects in the electric field by using simultaneously collected magnetic field data, aiming to address the distortion issues caused by static shift effects in the electric field and apparent resistivity. The method is validated through both theoretical models and field data, demonstrating its excellent correction performance. Additionally, the paper introduces the use of the multifractal spectrum analysis algorithm to analyze profile measurement points and study the fractal dimension characteristics of static shift effects, providing an effective way to evaluate the appropriateness and potential overcorrection of the correction. Finally, the multifractal features of field data are discussed, validating the ability of the multifractal spectrum to identify subsurface electrical complexity.

Keywords: time-frequency electromagnetic; static shift effect; multifractal spectrum analysis

1. Introduction

In electromagnetic exploration, the static shift effect is a phenomenon in which the presence of electrically heterogeneous bodies near the surface causes the accumulation of static charges on their surfaces due to the horizontal electric field, distorting the amplitude of the measured electric field and leading to a shift in apparent resistivity with logarithmic frequency, severely affecting the effectiveness of exploration [8,10,13].

To mitigate this effect, several methods have been developed, primarily falling into three categories: First, correction methods that incorporate prior information. For example, statistical variations in profile resistivity can be obtained through outcrop geology and resistivity measurements in the study area, or through statistical analysis of drilling data [8] and high-quality resistivity sounding curves [4,10,12,15]. However, such prior information is difficult to match perfectly with electromagnetic exploration areas and can be costly. Second, low-pass filtering methods. Since static shifts exhibit high-frequency characteristics, low-pass filtering can be applied to suppress such effects. The electromagnetic array profiling method, originally proposed by Bostick [4], uses spatial filtering for correction. Torres-Verdín and Bostick [17] analyzed the secondary magnetic field and electric field anomalies of shallow subsurface anomalies using the Born approximation method. However, spatial filtering methods are highly sensitive to the input parameters selected for the filter and heavily rely on the experience

 doi:10.20944/preprints202502.1721.v1

of data processors, often resulting in over- or under-correction, affecting exploration results. Third, correction using other data unaffected by static shifts. This involves using simultaneously collected electromagnetic data unaffected by static shifts, such as independently collected transient electromagnetic data [1,11,14,22], for correction, which has shown some effectiveness. Although this method avoids human interference, it requires independent acquisition systems, increasing workload and potentially being affected by survey point locations and acquisition parameters. Tournerie et al. [16] proposed a method to estimate apparent resistivity using the spatial distribution of phases, but this method requires at least 30 survey points and points not affected by static shift effects, making it unsuitable for independent or small-scale applications. To address these issues, this paper proposes a static shift correction method based on time-frequency electromagnetic (TFEM) data.

Time-frequency electromagnetic (TFEM) technology is a novel technique that combines time and frequency information for electromagnetic exploration [24,25]. Developed over more than two decades to meet the needs of oil and gas exploration transitioning from structural trap exploration to lithological and other hidden trap exploration, it has become a mature technology for oil and gas exploration and oil-bearing trap detection, widely applied with good exploration results [9,19,21,25,26]. TFEM technology simultaneously measures horizontal electric and vertical magnetic fields, leveraging the complementary advantages of electric and magnetic fields to enhance exploration effectiveness. However, current static shift correction methods in TFEM still use traditional filtering techniques, which may result in under- or overcorrection. To fully utilize the advantage of TFEM's simultaneous acquisition of vertical magnetic and horizontal electric fields for efficient static-shift correction, this paper proposes a new static shift correction method. Additionally, traditional static shift correction methods lack quantitative standards to judge the suitability of correction. To solve this problem, we introduce the fractal characteristic analysis.

Fractal characteristic analysis has been gradually applied to geophysical data analysis in recent years [2,5,18,20,23]. Multifractal analysis, which studies the global characteristics of a system from its local properties, mainly discusses the distribution laws of probabilities using statistical physics methods. Halsey et al. [6]proposed the mathematical framework for the multifractal spectrum, discussing the singularities of fractal measures and the mathematical foundation of multifractal analysis. We introduce this method to perform multifractal spectrum analysis on electric field data, analyzing the fractal dimension characteristics of static shift effects caused by shallow subsurface electrical heterogeneities, and further exploring the possibility of identifying geological anomaly features.

2. Materials and Methods

2.1. Principle of Static Shift Effects

The secondary field response of the shallow surface anomaly (x_0, y_0, z_0) in the far field case is used as an example to analyze the mechanism of the static shift effect. In electromagnetic exploration, the observed electromagnetic field can be written as the sum of the primary and secondary fields:

$$E = E_1 + E_2 \tag{1}$$

$$H = H_1 + H_2 \tag{2}$$

where E_0 and H_0 represent the primary field of the electric and magnetic fields, respectively, and E_2 represents the secondary field. Conductivity anomalies in the subsurface can be represented in a similar form:

$$\sigma = \sigma_0 + \Delta\sigma \tag{3}$$

where the uniform earth conductivity is σ_0, and the difference between the anomaly and the background conductivity is $\Delta\sigma$.

Under far-field conditions, the relationship between the electromagnetic fields can be described by a system of Maxwell's equations:

$$\nabla \times E = -i\omega\mu H \tag{4}$$

 doi:10.20944/preprints202502.1721.v1

$$\nabla \times H = \sigma E \tag{5}$$

where i is the imaginary unit, ω is the angular frequency of an electromagnetic wave, and μ is the magnetic permeability in a vacuum.

The Helmholtz equation for the secondary electric field can be obtained by substituting Equations (1)–(3) into (4) and (5):

$$\nabla^2 E_2 + i\omega\mu E_2 = i\omega\mu\Delta\sigma E \tag{6}$$

If $\Delta\sigma << \sigma$, the Helmholtz equations can be written in integral form with the help of Green's function, using the first-order Born approximation and replacing the total field with a primary field:

$$E_2(\vec{r}) = \int_v \Delta\sigma(r_0) G(r, r_0) E_1 e^{-ikz_0} dv \tag{7}$$

The above equation can be written as:

$$\frac{E_{2j}(\vec{r})}{E_1} = \int_v \rho_n(\vec{r}_0) K_{ej}(\vec{r}, \vec{r}_0) dv \tag{8}$$

The kernel function of the MT electric field orthogonal problem is:

$$K_{ej}(\vec{r}, \vec{r}_0) = -\Delta\sigma_0 G_j(\vec{r}, \vec{r}_0) E_1 e^{-ikz_0} \tag{9}$$

If the coordinates of the surface receiving point are $(x_0, y_0, 0)$, then it can be set:

$$K_{ej}(\vec{r}, \vec{r}_0) = \lambda_{ej}(x_0 - x, y_0 - y, z_0) \tag{10}$$

In the Cartesian coordinate system, equation(1.8) can be written as:

$$\frac{E_{2j}(\vec{r})}{E_1} = \int_0^\infty [\lambda_{ej}(x, y, z_0) * \rho_n(x, y, z_0)] dz_0 \tag{11}$$

where $*$ denotes a two-dimensional convolution about x and y. To obtain a more intuitive algebraic form, we perform a Fourier transform of the above equation to obtain the form in the wave number domain and set ξ, η, ζ to represent the wave number in the x, y, z direction, respectively.

$$\frac{E_j(\xi, \eta)}{E_1} = \int_0^\infty [\Lambda_{ej}(\xi, \eta, z_0) * P(\xi, \eta, z_0)] dz_0 \tag{12}$$

where $E_j(\xi, \eta)$ denotes the Fourier transform of $E_{2j}(\vec{r})$, Λ denotes the Fourier transform of λ, and $P(\xi, \eta, z_0)$ denotes the Fourier transform of $\rho_n(x, y, z_0)$. If $P(\xi, \eta, z_0)$ is regarded as the input and $\frac{E_j(\xi,\eta)}{E_0}$ as the output, Λ can be regarded as the transfer function of the linear system, and similarly, the linear integral equation of the quadratic magnetic field can be obtained in the wave number domain:

$$\frac{H_j(\xi, \eta)}{H_0} = \int_0^\infty [\Lambda_{hj}(\xi, \eta, z_0) * P(\xi, \eta, z_0)] dz_0 \tag{13}$$

The derivation process is omitted, and the electric-field Ex component transfer function is given directly:

$$\Lambda_{ex}(\xi, \eta) = \frac{i\omega\mu\sigma_0}{i\zeta} r_1(\xi, \eta) e^{-i(k+\zeta)z_0} + \frac{\xi^2}{i\zeta} e^{-i+(k\zeta)z_0} \tag{14}$$

The magnetic field H_z component kernel function is:

$$\Lambda_{hz}(\xi, \eta) = -\sqrt{i\omega\mu\sigma_0} r_2(\xi, \eta) e^{-i(k+\zeta)z_0} \tag{15}$$

Preprints.org (www.preprints.org) | NOT PEER-REVIEWED | Posted: 21 February 2025 doi:10.20944/preprints202502.1721.v1

where r_1, r_2 are parameters related to the wave number. Observation of the above equation shows that the electric field transfer function has two terms. The first term, which is frequency dependent, is referred to as the dynamic term and the second term, which is frequency independent, is the static term. For the anomaly with fixed depth z_0, the dynamic term for the data in the frequency domain varies with frequency ω, while the static term is the same for different frequency data, and the static term is the reason for the static shift effect. And equation (15) shows that there is no static term in the vertical component of the magnetic field, only a dynamic term. Thus, the magnetic field does not produce static shift effects.

2.2. Time-Frequency Electromagnetic Static Shift Correction Method

Using the fact that the magnetic field or magnetic induction components are not affected by the static shift effect, the electric field is corrected using apparent resistivity as an intermediary. The correction factor is initially derived by averaging the first three (or five) apparent resistivity values of the early magnetic field and the high-frequency electric field, respectively. This correction factor is then applied to the full frequency-domain data. Assuming a total of n measurement points, the specific method is outlined in Figure 1.

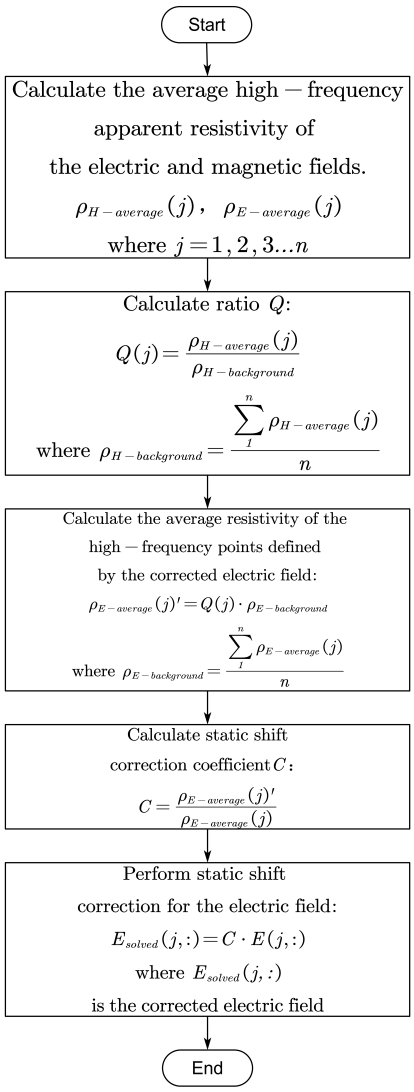

Figure 1. Flowchart of static shift correction.

 doi:10.20944/preprints202502.1721.v1

2.3. Multifractal Analysis of Electromagnetic Anomalies

Based on the theoretical analysis of static shift generation, it is evident that near-surface inhomogeneous conductivity bodies have different effects on the electric and magnetic fields. Therefore, we introduce the multifractal analysis method to distinguish the electric and magnetic field anomaly characteristics caused by near-surface inhomogeneous conductivity bodies.

Multifractals, also known as multiscale fractals, represent an advanced development of fractal theory in physics. The multifractal approach studies the overall characteristics of a system by examining its local features. Statistical physics methods are utilized primarily to discuss the distribution patterns of probability. The idea behind multifractal singularity spectrum analysis is to characterize the singularity properties of the normalized measure (distribution) defined on a fractal set, to express its scaling behavior. The singularity of the distribution is represented by the singularity strength α and the corresponding distribution density $f(\alpha)$. The multifractal spectrum is then determined by the range of values of α and the function $f(\alpha)$. In order to calculate the multifractal singularity spectrum of electromagnetic field data, the box-counting method [6] is used in this paper:

For any given set of 1D electromagnetic field data, denoted as X, we divide it into several boxes with a scale ε, covering the data. The probability measure of the normalized number of boxes $P_i(\varepsilon)$ is then spatially defined.

$$P_i(\varepsilon) = \frac{N_i(\varepsilon)}{N} \tag{16}$$

where N_i is the electromagnetic field data (mass, number of points) in the i-th box , and N is the total sum of the 1D electromagnetic field data (mass, number of points). As in $\varepsilon \to 0$, it can be assumed that the data are uniformly distributed across the boxes. For multifractal measures, for the i-th box on scale ε, P_i follows the following proportional relationship:

$$p_i(\varepsilon) \sim \varepsilon^{\alpha_i} \tag{17}$$

$$N_\alpha(\varepsilon) \sim \varepsilon^{f(\alpha)} \tag{18}$$

where α_i is the singularity scaling exponent and a partition function is defined as follows:

$$Z_q(\varepsilon) = \sum_{i}^{n_i(\varepsilon)} P_i^q \tag{19}$$

where $n_i(\varepsilon)$ is the number of boxes on the scale ε, and q is referred to as the weight factor. Its value can be arbitrary, but when $|q|$ reaches a certain level, further increases will no longer affect the multifractal spectrum.

Mass index:

$$\tau q = \lim_{\varepsilon \to 0} \frac{\log Z_q(\varepsilon)}{\log \varepsilon} \tag{20}$$

According to the Legendre transform, we can derive the multifractal singularity spectrum relationship for the electromagnetic field data:

$$f(\alpha_q) = q\alpha_q - \tau_q \tag{21}$$

$$\alpha_q = \frac{d\tau_q}{dq} \tag{22}$$

Taking α_q as the horizontal coordinate and $f(\alpha_q)$ as the vertical coordinate, the multifractal spectrum of the data from the electromagnetic field in 1D X can be obtained. The width of the multifractal spectrum, denoted as $\Delta\alpha$, is referred to as the inhomogeneity index:

$$\Delta\alpha = \alpha_{\max} - \alpha_{\min} \tag{23}$$

 doi:10.20944/preprints202502.1721.v1

For continuous and differentiable electromagnetic field data, $\Delta\alpha$ is a quantitative measure of the total rate of change (gradient) of all data points in the entire data set. Data that are not differentiable, such as apparent resistivity variations in electromagnetic methods, serve as the overall quantitative indicator of the data's inhomogeneity.

The width of the distribution density, denoted $f(\alpha)$, is referred to as the roughness index:

$$\Delta f(\alpha) = f(\alpha)_{\max} - f(\alpha)_{\min} \tag{24}$$

where $\Delta f(\alpha)$ represents the difference in the distribution density extrema of all data points within the entire electromagnetic field data. The smoother and more uniform the data, the smaller the roughness index.

The inhomogeneity index $\Delta\alpha$ and the roughness index $\Delta f(\alpha)$ are two key parameters that describe the multifractal characteristics of the data. When the electromagnetic field data do not exhibit multifractal characteristics, both $\Delta\alpha$ and $\Delta f(\alpha)$ are zero. The more pronounced the multifractal characteristics of the data, the larger the values of $\Delta\alpha$ and $\Delta f(\alpha)$.

3. Results

3.1. Example of Static shift Correction in a Theoretical Model

We design the 2.5D subsurface anomaly model Figure 2(a) and calculate its electromagnetic response Figure 2(c), and as a control, we first calculate the electromagnetic response of anomalies without a shallow surface Figure 2(b) and compare it with the results of the processing using this algorithm Figure 2(d).

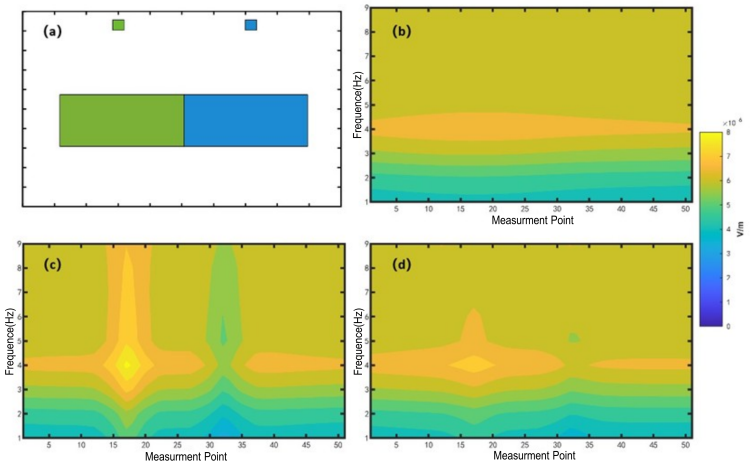

Figure 2. Simulation and correction of static shift in a theoretical model. (**a**) 2.5D geological structure profile, where green and blue represent high-resistivity and low-resistivity anomalies, respectively; (**b**) Theoretical forward response of the electric field without shallow anomaly bodies; (**c**) Forward response of the electric field with static shift effects; (**d**) Electric field response corrected using the proposed method.

It can be observed that the current algorithm effectively suppresses static shift, and the results closely match the theoretical results without static shift effects.

3.2. Example of Static Shift Correction on Measured Data

The time-frequency electromagnetic field measurement data Figure 3 from a specific region shows an apparent resistivity pseudo-section with a significant amount of longitudinal strip-like anomalies.

 doi:10.20944/preprints202502.1721.v1

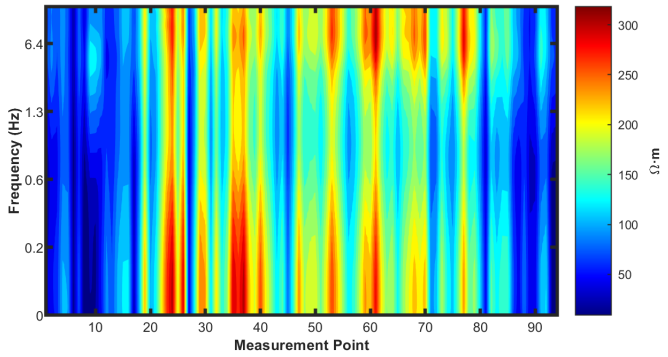

Figure 3. Pseudo-section of field data.

After processing with the algorithm proposed in this paper, the results shown in Figure 4 reveal significant changes in the electrical properties near the measurement points 10 to 17, which may correspond to regions with localized electrical property discontinuities in the subsurface. Near measurement point 65, there appears to be a noticeable low-resistivity layer. In the figure, it is evident that the proposed algorithm effectively eliminates most of the static shift, allowing the profile to clearly reflect the resistivity characteristics of the subsurface.

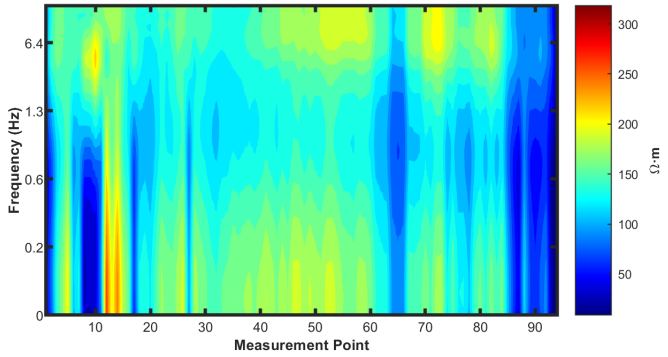

Figure 4. Pseudo-section after static shift correction.

3.3. Multifractal Spectrum Analysis of Electric Field in a Simple Electrical Model

Using the two parameters in the multifractal spectrum, we can distinguish deep anomalies that are obscured by static shift effects caused by shallow inhomogeneous bodies in the electric field data and also identify magnetic field anomalies induced by shallow anomalous bodies.

A 2.5D electrical profile model is designed as follows: The plate-like anomaly has the same depth as the upper surface of the shallow anomaly, and the resistivity is the same. The locations of the measurement points are shown in Figure 5, where the TM configuration is used to measure the electric field component E_x and the vertical magnetic field Hz. Figure 6 (a) shows the curve of the components of the electric field E_x component curve, and Figure 6(b) presents the multifractal spectrum.

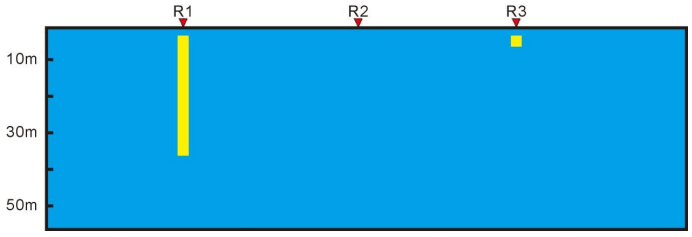

Figure 5. 2.5D profile of the geoelectric Model.

 doi:10.20944/preprints202502.1721.v1

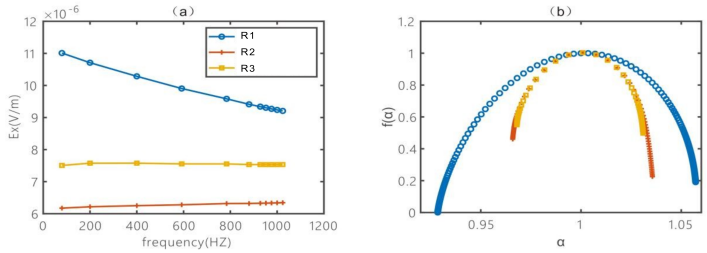

Figure 6. (**a**) Frequency-domain electric field E_x components measured at points R1, R2, and R3; (**b**) Multifractal spectra of the frequency-domain electric field E_x data at points R1, R2, and R3.

In the data of Figure 6(a), the electric field curves obtained at measurement points over the shallow subsurface anomaly and the vertical plate-shaped anomaly in the simple electrical model are quite similar in shape. In the presence of numerous shallow anomalies, the differentiation of them requires experience. In Figure 6(b), it can be seen that the multifractal spectrum of the shallow subsurface anomaly differs very little from the case without anomalies, indicating that the resistivity anomaly of the shallow subsurface anomaly manifests primarily as a static component effect. In contrast, the multifractal spectrum of the vertical plate-like anomaly shows significant differences, reflecting the presence of a true anomaly.

3.4. Multifractal Feature Analysis of Field Data

As previously discussed, the differences in multifractal spectra between shallow subsurface anomalies and plate-like anomalies substantiate that variations in the underlying anomalous bodies lead to different inhomogeneity and roughness characteristics in field data. We conducted a multifractal spectrum analysis on the field data before and after correction (Figure 3 and Figure 4). After correction, significant changes were observed in apparent resistivity values; however, the two multifractal scaling exponents exhibited minimal variation (Figure 7). This suggests that our static effect correction process effectively preserved the gradient variations between apparent resistivity values at different frequencies, along with information related to roughness and other inherent characteristics.

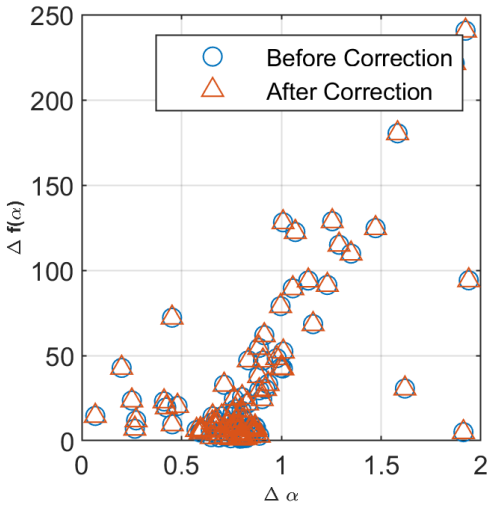

Figure 7. Comparison of multifractal spectra before and after correction.

By performing a multifractal spectrum analysis on the survey line (Figures 8 and Figure 9), it can be observed that the values at both ends of the line are significantly higher than those in the middle section, indicating that the complexity of the data is higher at the ends, suggesting more complex geological conditions. Although there are numerous longitudinal strip-like anomalies in the middle section, the broadly distributed and stable low values indicate that the anomalies in this segment of the profile are primarily caused by static shift effects.

Preprints.org (www.preprints.org) | NOT PEER-REVIEWED | Posted: 21 February 2025 doi:10.20944/preprints202502.1721.v1

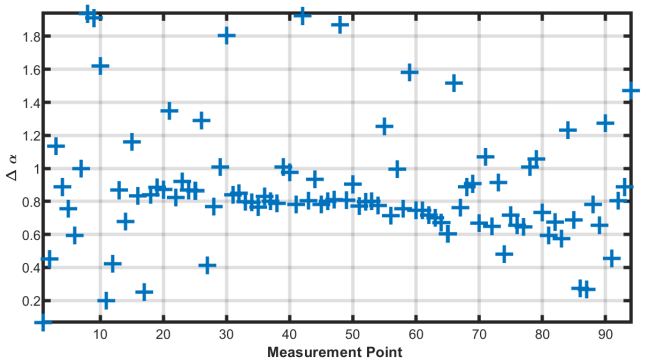

Figure 8. $\Delta\alpha$ at each measurement point in the field data.

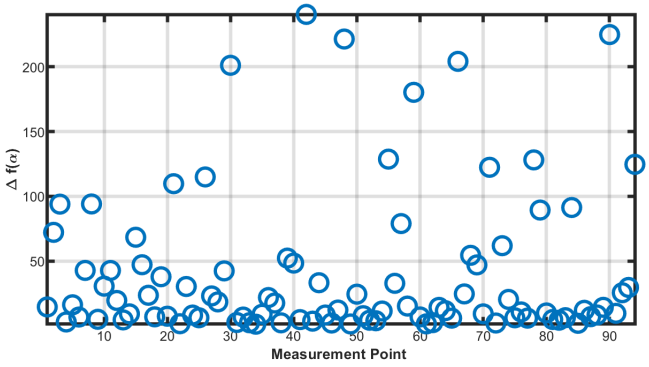

Figure 9. $\Delta f(\alpha)$ at each measurement point in the field data.

We also performed Gaussian mixture clustering in the multifractal spectrum, resulting in three categories of measurement points (Figure 10). The yellow regions are the most numerous and represent the most common data points in the profile. The cluster center of this region reflects the average data complexity of most of the measurement points. The points in the red region exhibit higher data complexity, indicating that the subsurface electrical structure beneath these points is more complex. In contrast, the points in the green region have very low complexity, suggesting a simpler subsurface electrical structure beneath these locations.

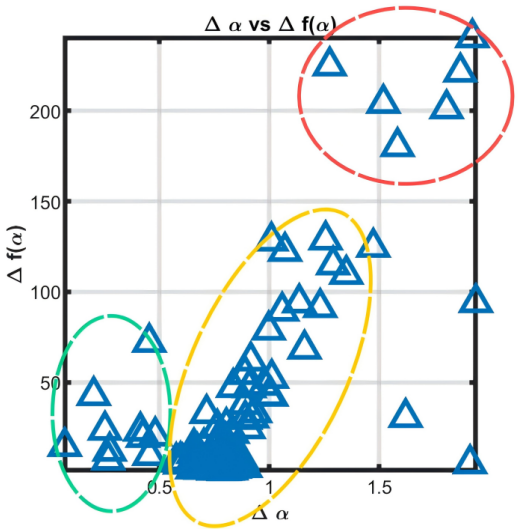

Figure 10. Clustering results of multifractal spectra for each measurement point in the field data.

In Figure 11, we marked the high-complexity and low-complexity measurement points, as identified by clustering, on the corrected apparent resistivity profile. Red indicates high-complexity data

 doi:10.20944/preprints202502.1721.v1

points, and green indicates low-complexity data points. It is clearly observed that the red dots correspond to areas with more significant electrical variations, while the green dots exhibit relatively small changes in both electrical properties and frequency. This shows that the multifractal spectrum effectively distinguishes the complexity of the subsurface electrical structure in the field data.

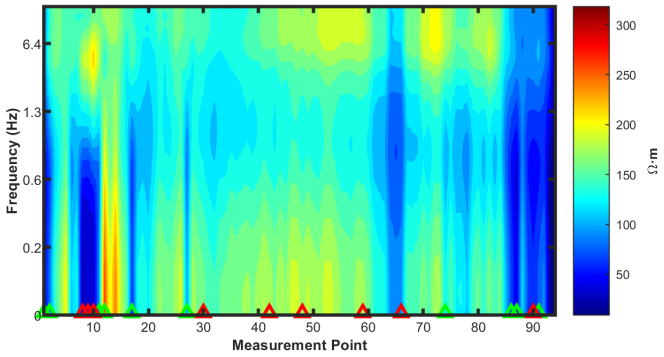

Figure 11. Measurement points with high complexity (red markers) and low complexity (green markers) as indicated by the multifractal spectra.

4. Discussion

From a mathematical perspective, the multifractal spectrum is highly sensitive to the overall gradient (inhomogeneity) and smoothness (roughness) of the data. The author envisions that this characteristic could be applied to geophysical inversion algorithms in the future. During the iterative solution process, not only would the measured data values be fitted, but also the multifractal spectrum of the forward response would be matched with that of the measured data. This approach could potentially improve both the efficiency and the accuracy of the inversion process. As inversion not only considers numerical restoration, but also requires the restoration of the relative relationships between the data. Multifractal spectrum analysis provides valuable insights for further data analysis.

5. Conclusions

We proposed a new time-frequency electromagnetic static shift correction method, taking advantage of the advantages of simultaneous measurement of electromagnetic fields in the time-frequency electromagnetic method. The apparent resistivity defined by the high-frequency magnetic field is used to correct the electric field. The method was validated using field data, demonstrating that our algorithm effectively eliminates the impact of static shift effects. In addition, we discussed the applicability of the multifractal algorithm in detecting the complexity of electromagnetic field data. We showed that, after static shift correction using this method, the changes in multifractal parameters are minimal, indicating that the method preserves the complete electrical information of the subsurface while correcting for static shift. Multifractal spectrum analysis can intuitively extract subsurface electrical complexity information from electrical field or apparent resistivity data, which not only evaluates the effectiveness of static shift correction from multiple dimensions but also provides important guidance for subsequent inversion processes.

References

1. Andrieux, P.; Wightman, W. Ed. The so-called static corrections in magnetotelluric measurements. In Proceedings of the SEG Technical Program Expanded Abstracts, 1984; 43–44.
2. Asrillah, A.; Abdullah, A.; Bauer, K.; Norden, B.; Krawczyk, C. M. Fracture characterisation using 3-D seismic reflection data for advanced deep geothermal exploration in the NE German Basin. *Geothermics* **2024**, *116*, 102833.
3. Bahr, K. Interpretation of the magnetotelluric impedance tensor: regional induction and local telluric distortion. *Journal of Geophysics* **1988**, *62*(1), 119–127.

 doi:10.20944/preprints202502.1721.v1

4. Bostick, F.X., Jr. Electromagnetic array profiling (EMAP). In Proceedings of the SEG Technical Program Expanded Abstracts, 1986; 60–61.
5. Gaci, S.; Nicolis, O. A grey system approach for estimating the hölderian regularity with an application to Algerian well log data. *Fractal and Fractional* **2021**, *5*(3), 86.
6. Halsey, T. C.; Jensen, M. H.; Kadanoff, L. P.; et al. Fractal measures and their singularities: The characterization of strange sets. *Physical Review A* **1986**, *33*(2), 1141.
7. He, Z.; Liu, X.; Qiu, W.; Zhou, H. Mapping reservoir boundary by borehole-surface TFEM: Two case studies. *The Leading Edge* **2005**, *24*(9), 896–900.
8. Jones, A. G. Static shift of magnetotelluric data and its removal in a sedimentary basin environment. *Geophysics* **1988**, *53*(7), 967–978.
9. Li, Z. Q.; Fu, G. Q.; Tan, S. Q.; Chen, X. G.; Guo, T.; Xiang, P.; ...; He, Z. X. Calculation and application of apparent resistivity in the frequency domain by TFEM. *Applied Geophysics* **2024**, *21*(2), 409–417.
10. Ogawa, Y. On two-dimensional modeling of magnetotelluric field data. *Surveys in Geophysics* **2002**, *23*, 251–273.
11. Pellerin, L.; Hohmann, G. W. Transient electromagnetic inversion: A remedy for magnetotelluric static shifts. *Geophysics* **1990**, *55*(9), 1242–1250.
12. Schultz, A.; Kurtz, R. D.; Chave, A. D.; Jones, A. G. Conductivity discontinuities in the upper mantle beneath a stable craton. *Geophysical Research Letters* **1993**, *20*(24), 2941–2944.
13. Singer, B. S. Correction for distortions of magnetotelluric fields: limits of validity of the static approach. *Surveys in Geophysics* **1992**, *13*, 309–340.
14. Sternberg, B. K.; Washburne, J. C.; Pellerin, L. Correction for the static shift in magnetotellurics using transient electromagnetic soundings. *Geophysics* **1988**, *53*(11), 1459–1468.
15. Tournerie, B.; Chouteau, M. Analysis of magnetotelluric data along the Lithoprobe seismic line 21 in the Blake River Group, Abitibi, Canada. *Earth, Planets and Space* **2002**, *54*, 575–589.
16. Tournerie, B.; Chouteau, M.; Marcotte, D. Magnetotelluric static shift: Estimation and removal using the cokriging method. *Geophysics* **2007**, *72*(1), F25–F34.
17. Torres-Verdin, C.; Bostick, Jr., F. X. Implications of the Born approximation for the magnetotelluric problem in three-dimensional environments. *Geophysics* **1992**, *57*(4), 587–602.
18. Turcotte, D. L. *Fractals and Chaos in Geology and Geophysics*, 2nd ed.; Cambridge University Press: Cambridge, UK, 1997.
19. Weibin, D.; Xiaoming, Z.; Fang, L.; Guo, Z. The time-frequency electromagnetic method and its application in western China. *Applied Geophysics* **2008**, *5*(2), 127–135.
20. ZENG, X.; LIU, T.; TAN, X.; ZHANG, Y.; LI, X. Automatic determination of the cut-off wavenumber for downward continuation of potential field based on fractal radial spectrum. *Progress in Geophysics* **2024**, *39*(1), 403–411.
21. ZHANG, C. H.; LIU, X. J.; HE, L. F.; HE, W. H.; ZHOU, Y. M.; ZHU, Y. S.; ...; KUANG, X. H. A study of exploration organic rich shales using Time-Frequency Electromagnetic Method (TFEM). *Chinese Journal of Geophysics* **2013**, *56*(9), 3173–3183.
22. Zhang, P.; Chouteau, M.; Mareschal, M.; Kurtz, R.; Hubert, C. High-frequency magnetotelluric investigation of crustal structure in north-central Abitibi, Quebec, Canada. *Geophysical Journal International* **1995**, *120*(2), 406–418.
23. Zhang, X.; Li, D.; Li, J.; Liu, B.; Jiang, Q.; Wang, J. Signal-noise identification for wide field electromagnetic method data using multi-domain features and IGWO-SVM. *Fractal and Fractional* **2022**, *6*(2), 80.
24. Zhanxiang, H.; Zhi, Z.; Haiying, L.; Jinchen, Q. TFEM for oil detection: Case studies. *The Leading Edge* **2012**, *31*(5),
25. Zhanxiang, H.; Xiaodong, S.; Zuzhi, H.; Yanling, S.; Dongyang, S.; Weibin, D. Time–frequency electromagnetic method for exploring favorable deep igneous rock targets: A case study from north Xinjiang. *Journal of Environmental and Engineering Geophysics* **2019**, *24*(2), 215–224.
26. Zhao, Z.; He, Z.X.; Li, D.C.; Yang, S.J.; Liu, X.J.; Li, T.B. Detecting favorable oil and gas targets with time-frequency electromagnetic method–case studies. In *Proceedings of the 72nd EAGE Conference and Exhibition incorporating SPE EUROPEC 2010*, Amsterdam, Netherlands, 23–26 June 2010; cp–161.

 doi:10.20944/preprints202502.1721.v1

disclaim responsibility for any injury to people or property resulting from any ideas, methods, instructions or products referred to in the content.